J Mater Sci (2012) 47:2932–2942
DOI 10.1007/s10853-011-6126-z

In-plane conduction of polymer composite plates reinforced with architectured networks of Copper fibres

Laurent Orgéas · Pierre J. J. Dumont · Jean-Pierre Vassal · Olivier Guiraud · Véronique Michaud · Denis Favier

Received: 16 September 2011 / Accepted: 11 November 2011 / Published online: 29 November 2011

Abstract Model composite plates composed of highly conductive slender copper fibres impregnated with a poorly conductive and transparent PMMA matrix were processed with different fibrous architectures, i.e. with various controlled fibre contents and orientations. Their microstructure was characterised using both optical observations and X-ray microtomography. Their in-plane thermal conductivity was measured by using a specific testing apparatus combined with an inverse modelling method. Results point out the strong link between the anisotropy of the in-plane conductivity and of the microstructure. The role of the fibre content on the conductivity is also emphasised. An analytical conduction model which accounts for the influence of the fibre content, the orientation, the aspect ratio and the thermal resistances at fibre-fibre contacts, was proposed and its predictions were compared with the experimental results. Using only one fitting parameter, namely the conductance at fibre-fibre contacts, this model shows a good prediction of all the experiments.

This study was performed within the ANR research program "3D discrete analysis of deformation micro-mechanisms in highly concentrated fiber suspensions" (ANAFIB, ANR-09-JCJC-0030-01). J. P. Vassal and O. Guiraud would like to thank the Région Rhône-Alpes (France) and the competitiveness cluster Plastipolis (France) for their research grants.

L. Orgéas (✉) · J.-P. Vassal · O. Guiraud · D. Favier
CNRS/Université de Grenoble, Laboratoire Sols-Solides-Structures-Risques (3SR), BP 53, 38041 Grenoble cedex 9, France
e-mail: Laurent.Orgeas@grenoble-inp.fr

P. J. J. Dumont · O. Guiraud
CNRS/Institut Polytechnique de Grenoble, Laboratoire de Génie des Procédés Papetiers (LGP2), BP 65, 38402 Saint-Martin-d'Hères cedex, France

V. Michaud
École Polytechnique Fédérale de Lausanne (EPFL), Laboratoire de Technologie des Composites et Polymères (LTC), Station 12, CH 1015 Lausanne, Switzerland

Introduction

Increasing thermal or electrical conductivity of fibrous materials such as polymer composites by using a high content of slender conductive particles, e.g. short carbon fibres [20], carbon nanotubes [10, 22] or short and/or entangled metallic fibres [9, 11, 12, 39], could provide a lightweight technological solution in many applications and components such as heat or electrical exchangers, Faraday's electrical barriers, electrical batteries. Most of these components have a shell-like geometry, where fibres are connected and mainly orientated within the shell's midplane. Their in-plane thermal or electrical conductivity has to be optimised with respect to the architecture of their fibrous reinforcement. However, an important limitation in the development of such functionalised materials is the difficulty to predict their effective in-plane conductivity.

A first reason is the lack of analytical conductivity models. Indeed, if conduction phenomena in heterogenous materials have been studied for several decades [19, 28, 41, 36], the prediction of the conductivity in connected and conductive fibrous media still remains an open question. Owing to the high-conductivity contrast between the fibrous networks and their surrounding matrix, predictions given by standard bounds may be inaccurate [7, 21, 46, 48]. Thus, other theories have been developed for composites with a low content of highly conductive fibres, i.e. far below the percolation threshold [34]. They still cannot properly account for fibre-fibre interactions

occurring at contact points when the composites are composed of connected fibres [37]. In parallel, numerical estimations have been proposed in the concentrated regime where the fibrous networks are considered as an assembly of connected resistors and where conduction within the surrounding matrix is usually neglected [8–10, 17, 18, 23, 29, 45, 47] except in some studies, e.g. [37]. Purely analytical models for similar situations are scarce [2, 45, 47]. They are restricted to particular fibre orientations, they do not account for conduction in the matrix, and they are valid for good or poor fibre contacts (the intermediate situation is not modelled). More recently, by extending concepts initially introduced for conductive granular materials [6], analytical conductivity models for highly concentrated fibrous media with possible fibre–fibre interface barriers were proposed [42–44]. Depending on the quality of fibre–fibre contacts, three equivalent continua were identified, i.e. when the fibre–fibre conduction through contacts is very good, poor, or of the same order of magnitude than that occurring inside the fibres, respectively. Analytical conduction models could be established in the case of slender, straight, monodisperse and homogeneously distributed fibres. These models are restricted to very high-conductivity ratios between the fibres and the surrounding matrix, typically above 10^4–10^6. Unfortunately, their predictions have not been compared to experimental data yet.

A second reason is the lack of reliable experimental results obtained by using fibrous materials with well-controlled and well-characterised fibrous architectures. Indeed, the model predictions are usually compared with experimental data measured on thin plate samples produced under industrial processing conditions. First, the microstructures of the as-processed composites are difficult to control and may exhibit strong heterogeneities through the thickness and the midplane of produced plates [11, 12, 25], inducing large experimental scattering. As a result, the model validation becomes sometimes questionable. Second, process-induced fibrous microstructures are often difficult to observe and characterise, due to the size and the shape of the fibres, their high-concentration required to reach the prescribed conductivity (i.e. largely above the percolation threshold), and/or the opaque nature of polymers that are generally used. This is really disturbing since conduction phenomena in such materials highly depend on the geometry, the content and the orientation of the fibres and of the fibre–fibre contact areas. A first approach to overcome this difficulty is to use model composites with a transparent matrix where direct 2D optical observations are possible [14, 31, 49]. When the fibrous reinforcement and the matrix properties make it possible, X-ray microtomography also appears as a very relevant characterisation technique [15, 16, 24, 25, 27, 35].

Therefore, this study aims at (i) proposing a model for the in-plane conductivity of some composite plates or shells made up of conductive fibres based on the previously presented models and (ii) comparing its predictions with measurements of the thermal in-plane conductivity of composite plates, the fibrous architecture of which was controlled during the processing and finely characterised using 2D direct observations and X-ray microtomography.

Theoretical background

We consider the conduction inside a composite reinforced by slender fibres of length l_f and with circular cross section of diameter d_f such that the fibre aspect ratio $r = l_f/d_f \gg 1$. The matrix and fibre conductivities λ_m and λ_f are such that $\lambda_f \gg \lambda_m$. Within the low or dilute concentration regime d, i.e. when r and/or the volume fraction of fibres ϕ are sufficiently small, there is no fibre-fibre contact: the slender conductive fibres act as source elements that enhance transport phenomena in the matrix, provided that the conduction at fibre-matrix interfaces is good. Within the concentrated regime c, i.e. at high r and/or high ϕ values, fibre–fibre contacts form in the composite and lead to additional transport mechanisms in contact zones of typical contact surface S_c and conductance h_c.

In practice, it may be difficult to neglect a priori one of the mentioned conduction mechanisms, i.e. conduction within the matrix and the fibres (the main mechanisms in the dilute regime d) and conduction within the fibres and through the fibre–fibre contacts (the main mechanisms in the concentrated regime c). Thus, it would be useful to have an analytical model which could account for all cases into a proper expression of the macroscopic/effective conductivity tensor $\mathbf{\Lambda}$ of the composites under consideration. Thus, by taking into account the linearity of the local transport mechanisms, it is assumed that $\mathbf{\Lambda}$ can be split into two contributions, i.e.

$$\mathbf{\Lambda} \approx \mathbf{\Lambda}^{d} + \mathbf{\Lambda}^{c}, \tag{1}$$

where the conductivity tensors $\mathbf{\Lambda}^{d}$ and $\mathbf{\Lambda}^{c}$ account for the two mentioned local conduction mechanisms, respectively.

In the absence of fibre–fibre contacts, Rocha and Acrivos [34] proposed estimations of the conductivity tensor $\mathbf{\Lambda}^{d}$. In the case where the conductivity contrast between the fibres and the surrounding matrix is high and the fibres are straight and very slender, $\mathbf{\Lambda}^{d}$ can be simply expressed as

$$\mathbf{\Lambda}^{d} = \lambda_m \left(\boldsymbol{\delta} + \frac{2\phi r^2}{3 \ln 2r} \mathbf{A} \right), \tag{2}$$

where $\mathbf{A}$ is the second-order fibre orientation tensor [1], for which a discrete expression can be obtained from the knowledge of the orientation of the N fibres i of unit vectors $\overline{\mathbf{p}}^{i}$ contained in a representative volume [14, 26]:

$$\mathbf{A} = \frac{1}{N}\sum_{i=1}^{N} \overline{\mathbf{p}}^i \otimes \overline{\mathbf{p}}^i. \tag{3}$$

Several comments can be made regarding Eq. 2:

- As ϕ tends to 0, $\mathbf{\Lambda}^{\mathrm{d}}$ tends to the conductivity $\Lambda_{\mathrm{m}}\boldsymbol{\delta}$ of the matrix.
- $\mathbf{\Lambda}^{\mathrm{d}}$ is an affine function of the volume fraction of fibres ϕ. This trend, only valid within the dilute concentration regime, is not in accordance with most of the experiments (see for instance [2, 10, 39], where a departure from the linear dilute regime is observed as the fibre content and/or aspect ratio increase towards the concentrated regime).
- As r and/or ϕ increase, the first term of the right-hand side of Eq. 2 becomes rapidly negligible in case of slender fibres and $\mathbf{\Lambda}^{\mathrm{d}}$ becomes a linear function of the fibre orientation tensor $\mathbf{A}$. Written in the principal axes $\mathbf{e}_i (i = \mathrm{I}, \mathrm{II}, \mathrm{III})$ of $\mathbf{A}$, this implies that the ratios $\Lambda_i^{\mathrm{d}}/A_i (i = \mathrm{I}, \mathrm{II}, \mathrm{III}$, no summation on the indice i) do not depend on the indice i.
- This expression considers fibres as very slender bodies and does not account for fibre conduction perpendicular to the fibre centre lines (more sophisticated expressions could be used, see Rocha and Acrivos [34]). Thus, in some situations, it underestimates the conductivity. This is the case for the conductivity perpendicular to networks of fibres with planar fibre orientation, such as those considered in this study. However, as this study mainly focuses on the in-plane conductivity of the fibrous shells or plates (see the introduction), Eq. 2 is relevant enough and will be used in the following.

When the fibre connectivity becomes pronounced and when the conductivity contrast between the fibres and the matrix is very high, conduction phenomena inside the matrix can be neglected as a first approximation [6]. Then, conduction only occurs inside the fibres and through contact zones. The local equilibrium of the considered fibrous media is ruled by a dimensionless Biot number $\mathbb{B}$, which can be expressed as

$$\mathbb{B} = \frac{4h_{\mathrm{c}}l_{\mathrm{f}}}{\pi\bar{Z}\lambda_{\mathrm{f}}}\varphi_3 \tag{4}$$

in the case of straight, short, monodisperse and homogeneously distributed fibres with circular cross sections [44]. In this expression, $\bar{Z}$ is the average fibre coordination number, i.e. the average number of fibre-fibre contacts per fibre. The fibre orientation descriptor φ_3 represents the average of the inverse of the sine of the angles between contacting fibres (see Eq. 9c), so that the more aligned the contacting fibres, the larger their contact surface, the larger the heat transfers in this zone and the larger the Biot number.

Depending on $\mathbb{B}$, three conduction models arise [42, 43]. For high Biot number (model I), the physics at the fibre scale is ruled by conduction within fibres. Conversely, for low Biot number (model III), this physics is ruled by conduction through fibre-fibre contacts and the effective conductivity only depends on the conductance h_{c}. Model II covers the intermediate case. As a rule of thumb, in models I and III, the overall conduction is governed by the property of the structural features (fibre segments or contacts) which hinders it. In case of straight, monodisperse and homogeneously distributed fibres with circular cross sections, expressions $\mathbf{\Lambda}^{\mathrm{cI}}$ and $\mathbf{\Lambda}^{\mathrm{cIII}}$ of $\mathbf{\Lambda}^{\mathrm{c}}$ can be obtained for models I and III by using slender body approximations [43, 44]:

$$\mathbf{\Lambda}^{\mathrm{cI}} = \phi\lambda_{\mathrm{f}}\left(1 - \frac{1}{\bar{Z}}\right)\mathbf{A} \tag{5}$$

$$\mathbf{\Lambda}^{\mathrm{cIII}} = \bar{Z}\phi h_{\mathrm{c}}\varphi_3\frac{l_f}{3}\left(1 - \frac{1}{\bar{Z}}\right)\mathbf{A}. \tag{6}$$

For model II, it was not possible to establish an analytical expression. However, by using discrete element simulation, a phenomenological analytical expression of $\mathbf{\Lambda}^{\mathrm{c}}$ was proposed when r ranges from 5 to 100, ϕ ranges from 0.02 to 0.4, and the conductivity ratio $h_{\mathrm{c}}/\lambda_{\mathrm{f}}$ ranges from 1 to 10^9 m^{-1} [44]:

$$\mathbf{\Lambda}^{\mathrm{c}} \approx \frac{1}{2(1 + 10\bar{Z}\phi\mathbb{B})}\left(\mathbf{\Lambda}^{\mathrm{cIII}} + 10\bar{Z}\phi\mathbb{B}\mathbf{\Lambda}^{\mathrm{cI}}\right). \tag{7}$$

- This expression tends to the analytical expressions (5) obtained for models I and III as $\mathbb{B}$ tends to ∞ or 0, respectively.
- In order to estimate the coordination number $\bar{Z}$ and the orientation descriptor φ_3, [43] suggested to use the statistical geometrical tube model [13, 33, 40]:

$$\bar{Z} = 4\phi\left(\frac{2}{\pi}r\varphi_1 + \varphi_2 + 1\right) \tag{8}$$

where [14, 26]

$$\begin{cases} \varphi_1 = \frac{1}{N^2}\sum_{i=1}^{N}\sum_{k=1}^{N}||\overline{\mathbf{p}}^i \times \overline{\mathbf{p}}^k|| \\ \varphi_2 = \frac{1}{N^2}\sum_{i=1}^{N}\sum_{k=1}^{N}|\overline{\mathbf{p}}^i \cdot \overline{\mathbf{p}}^k| \\ \varphi_3 = \frac{1}{N^2}\sum_{i=1}^{N}\sum_{k=1}^{N}\frac{1}{||\overline{\mathbf{p}}^i \times \overline{\mathbf{p}}^k||} \end{cases} \tag{9}$$

This simple microstructural model assumes that fibres are straight, spatially uniformly distributed and can overlap (softcore assumption). In the following, its validity will be investigated.

- For high values of the Biot number, i.e. for good to very good contacts, the ratios $\Lambda_i^{\mathrm{c}}/A_i$ become independent of the fibre orientation, as already mentioned for the ratios

Λ_i^d/A_i. This remark still holds at lower Biot numbers, when comparing fibrous architectures with different fibre orientations but with nearly identical values of φ_3 (see Sect. 4)

- For very good contacts ($\mathbf{\Lambda}^c \approx \mathbf{\Lambda}^{cI}$) and when $(1 - 1/\bar{Z}) \approx 1$, the model predicts an affine increase of the conductivity with the fibre content ϕ. Similarly, in case of very poor contacts ($\mathbf{\Lambda}^c \approx \mathbf{\Lambda}^{cIII}$), a quadratic increase of the conductivity with ϕ is expected.
- As for the dilute case, even if more sophisticated models could have been established [43], some of the slender bodies assumptions were stated to simplify the analytical expressions. For example, in the case of the models I and II, the temperature of the fibre centrelines in front of a contact was assumed to be identical to the fibre temperature near the contact zone. The model can then underestimate the conductivity in some situations, e.g. conduction perpendicular to networks of fibres with planar fibre orientations: such situations are different from those considered in this study.

Consequently, if the conductivities of the fibres and the matrix together with the fibrous architecture of the composite plates are known (see next sections), it is important to point out that the analytical model (1, 2, 5, 7) only requires one unknown parameter to be identified, i.e. the contact conductance h_c.

Experimental procedure

Materials and processing conditions

In order to check the validity of the previous conductivity estimation, model composite plates made up of a poorly conducting polymer matrix reinforced with highly conducting slender and rather straight fibres with controlled architectures were processed:

- Straight copper fibres having a circular cross section of diameter $d_f = 0.2\text{mm}$ and a length $l_f = 10\text{mm}(r = 50)$ were cut from standard electric wires. They were chosen because of their stable thermophysical properties between 20 and 40 °C (i.e. the temperature range of the experiments) and their high thermal conductivity (see Table 1).
- A PMMA matrix (Altuglas, Atofina) was chosen. Firstly, between 20 and 40 °C, its thermophysical properties exhibit very weak variations ([3], see Table 1). Besides, its low thermal conductivity induces a rather high-conductivity ratio $\lambda_f/\lambda_m \approx 2100$. Lastly, its transparency allows the fibrous architectures of the processed composite plates to be easily characterised.

Table 1 Thermophysical properties of the PMMA matrix [3] and the copper fibres between 20 and 40 °C

	Thermal conductivity ($\text{Wm}^{-1}\ \text{K}^{-1}$)	Volumetric specific heat ($\text{kJ m}^{-3}\ \text{K}^{-1}$)
PMMA	$\lambda_m \approx 0.19$	$1610 \leq \rho_m C_m \leq 1710$
Copper	$\lambda_f \approx 400$	$\rho_f C_f \approx 3450$

To obtain plates with (i) homogeneously distributed fibres and controlled fibre content and orientation, and (ii) similar characteristic contact conductance h_c, the processing route proposed in Dumont et al. [14] was adopted and a special attention was paid to subject the samples to the same thermo-hygro-mechanical conditions:

- Prescribed quantities of copper fibres and PMMA powder (the PMMA was delivered as a granular powder with an average grain size about 0.05 mm) were forced to fall into a vertical channel down to a cylindrical mould of diameter 120 mm. During this fall, the fibres and the powder went through a series of 10 equally spaced (vertical distance 30 mm) horizontal grids of metallic thin wires with regular square holes of dimensions $30 \times 30\ \text{mm}^2$. The spatial position and orientation of the holes were random, allowing a homogeneous distribution and a random orientation of the fibres in the principal plane of the mould to be obtained. To process samples with a preferred fibre orientation, a last grid made up of parallel metallic thin wires (distance between them $< l_f$) was added.
- The as-processed thin cakes were first dried in a oven for 1 h at 120 °C in order to evaporate the possible entrapped water from the PMMA. Then they were compressed in the mould for 2 h at the same prescribed packing stress of 0.177 MPa and to the same temperature of 220 °C. During this stage, the PMMA was compacted. Resulting cylindrical plates (diameter of 120mm, thickness of 3.5mm) exhibited no pores and nearly 2D planar fibrous microstructures.
- Lastly, in order to avoid microstructural boundary effects, rectangular samples ($66 \times 66 \times 3.5\ \text{mm}^3$) were cut from the centres of the processed plates, their edges being parallel with the principal axes of the fibre orientation.

Seven rectangular plates were processed, with volume fractions of copper fibres ϕ ranging from 0.02 to 0.24 and two different fibre orientations, i.e. a nearly planar random fibre orientation (three samples) and a preferred fibre orientation along the $\mathbf{e}_1$-direction (four samples).

Microstructure observations

Two types of observations were performed because of the large absorption contrast between the materials of the

composite plates. The first one was direct 2D optical observation. The second one was the X-ray microtomography (RX solution, 3SR Lab, Grenoble, France, scans achieved with 1500 X-ray 2D radiographs onto a 1914 × 1580 pixels CCD detector, voxel size = 10 × 10 × 10 μm^3): it was achieved on two small specimens cut from two different plates, i.e. one with orientated fibres and $\phi = 0.17$, the other with a planar random fibre orientation and $\phi = 0.10$. After suitable reconstruction and thresholding, 3D binary representations of the fibrous architectures could be obtained.

Measurement of the in-plane conductivities

There are different techniques which aim at measuring the thermal conductivity of fibre reinforced composites [4, 30, 32, 38]. Among them, a method which constitutes a good compromise between its accuracy and its simplicity was chosen. Hence, the method proposed by Sweeting and Liu [38] was used in order to estimate the components Λ_{11} and Λ_{22} of the effective conductivity tensor $\mathbf{\Lambda}$ of the plates along their midplanes ($\mathbf{e}_1$, $\mathbf{e}_2$):

- Each sample was first subjected to a one-dimensional transient heat flow. This was achieved with a specially designed testing apparatus schematically shown in Fig. 1a. Such a setup ensures that lateral heat losses occurring during the experiments could be considered as negligible. For that purpose, heat losses were reduced (i) by making experiments in a primary vacuum so that convection was limited and (ii) by adding a reflecting layer (thin metallic sheet) on the insulating walls of the apparatus so that radiation loss was limited (see Fig. 1a). In the initial state, the whole setup and the tested sample were at the same constant temperature, i.e. 20 °C. Then, the lower and upper faces of the sample were subjected to a thermal difference of 30 °C using thermally regulated water at $T^- = 20$ °C and $T^+ = 50$ °C, respectively (see Fig. 1a).
- Second, the temperatures inside the sample were recorded at different locations along the vertical heat flow direction. This was achieved with 4 equally spaced thermocouples P_i (see Fig. 1a, distance between two adjacent thermocouples $\Delta h = 10$ mm). A typical time evolution of the temperatures T_i given by the thermocouples P_i is shown in Fig. 1b.
- Third, an inverse numerical approach was used. A 1D thermal model of the experiment was built with the finite element code Comsol 3.4. More precisely, the standard heat balance equation

$$\rho C \partial T/\partial t = \Lambda \partial^2 T/\partial x^2 \tag{10}$$

was discretised and solved along the length of the tested sample, the experimental data T_1 and T_4 recorded by the lowest and the highest thermocouples P_1 and P_4 were used as time-evolving boundary conditions, and the volumetric heat capacity ρC involved in the heat equation was estimated by a volume average [5]. For the sake of simplicity, ρC was assumed to be temperature independent: such an assumption may induce a very small difference (less than 5%) on the estimation of Λ compared with calculations which would have accounted for the small variation of the volumetric heat capacity $\rho_m C_m$ of the PMMA ([3], see Table 1). An optimisation algorithm which was implemented in Matlab was used to compute the value of the effective conductivity Λ that minimised the error between the experimental and the numerical temperatures T_2 and T_3 of the two central thermocouples P_2 and P_3. This optimisation was carried out by following the Nelder Mead algorithm used for multi-dimensional unconstrained non-linear minimisation. As an example, we have reported in Fig. 1b the best fit (red continuous lines) of experimental data (marks) obtained by the optimisation: the numerical fit is fairly good.

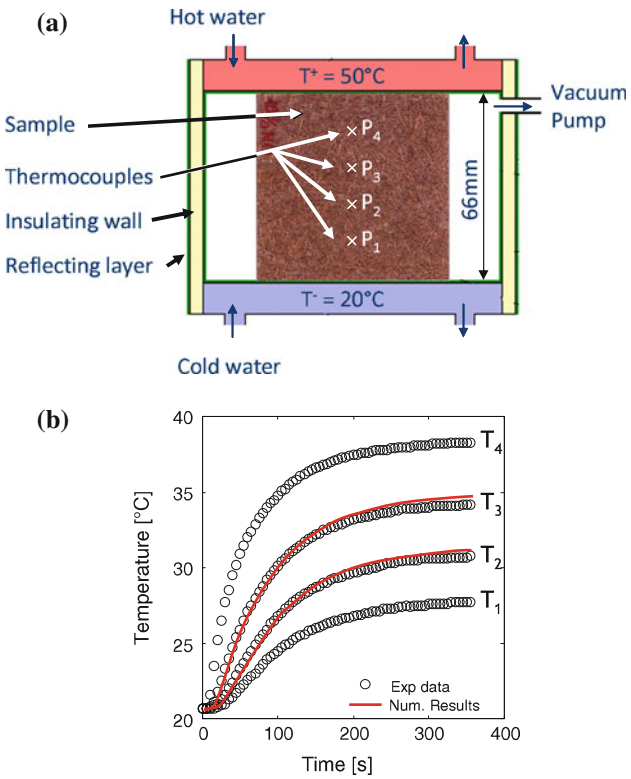

Fig. 1 Scheme of the experimental device used to estimate the in-plane conductivities (**a**), and example of data obtained during an experiment (*marks*) together with the calculations (*continuous lines*) deduced from the inverse modelling (**b**) (orientated sample, $\phi = 0.17$, the principal direction of fibres being aligned with the flow direction)

- This measure was performed along the two in-plane directions $\mathbf{e}_1$ and $\mathbf{e}_2$ of the fibre orientation in order to obtain the in-plane components, respectively, Λ_{11} and Λ_{22}, of the effective thermal conductivity tensor.

By repeating the measurements, i.e after remounting the tested plates in the apparatus (i) in the same position or (ii) by rotating them with an angle of 180° around $\mathbf{e}_3$ with respect to its initial position, the relative error on the estimated thermal conductivity was found to be close to ±15%. On the one hand, this scattering is larger than what is observed with plates made up of a homogeneous one phase material, i.e ≈±3% [38]: this is mainly ascribed to small spatial and local heterogenities of the processed fibrous networks. On the other hand, as seen in the following, the ±15% scattering observed on the conductivity results is sufficiently small so that trends induced by the considered variations of the architecture of the fibrous networks can be easily observed and discussed.

Characterisation of the fibrous architectures

As a qualitative example, the 2D micrographs (a–d) in Fig. 2 provide optical top views (a, b) and lateral views (c, d) of two produced plates with a volume fraction of fibres $\phi = 0.1$. The first sample (Fig. 2a, d) exhibits a nearly 2D planar random fibre orientation, and the second one (Fig. 2b, c) a noticeable fibre orientation along the $\mathbf{e}_1$-direction. The rather good in-plane (Fig. 2a, b) and out-of-plane (Fig. 2c, d) homogeneity of produced samples is also qualitatively observed here. Similar qualitative conclusions can be drawn from the 3D X-ray micrograph (a) displayed in Fig. 3. Quantitative data on the fibrous microstructures (fibre location, geometry and orientation, contact location and orientation) were obtained with additional image analysis operations, by using the softwares ImageJ, Avizo and Matlab. They are summarised in Fig. 3 in the case of the 3D scanned volumes.

– Fibre centreline and orientation—To detect the centreline of each fibre contained inside the scanned volumes (i.e. to obtain Fig. 3b from Fig. 3a), a 3D distance map was first calculated inside the fibrous phase from the segmented volumes. A thresholding operation was then carried out by using the resulting volume, in order to separate contacting fibres. Then, a standard 3D skeletonisation algorithm was used in order to estimate the position and the geometry of the fibre centrelines, which were finally smoothed and labelled. Thereby, it was possible to estimate the tortuosity of each fibre, defined as the length of the fibre centreline divided by the chord joining the two extremities of the same centreline: the average value of this tortuosity was found to be equal to 1.0045 (in the example of Fig. 3b), i.e very close to 1. Consequently, within the processed plates, each fibre i can be considered as straight enough to be assigned a unique mean orientation vector $\overline{\mathbf{p}}^i$, defined as the unit vector parallel to the minor inertial axis of the fibre i. It was then possible to quantify the fibre orientation in the composite plates, as shown in the example of Fig. 4a. In this figure, spots plotted on the surface of the unit sphere represent the extremities of the N orientation vectors $\overline{\mathbf{p}}^i$ ($N = 133$ in the example given in Fig. 3), their origin being located at the centre of the sphere. The second-order fibre orientation tensor $\mathbf{A}$ together with the orientation functions φ_1, φ_2 and φ_3 are also given in the figure. These parameters were obtained from the discrete expressions given by Eqs. 3, 9. First, the nearly zero non-diagonal components of $\mathbf{A}$ prove that the reference frame of the plates ($\mathbf{e}_1$, $\mathbf{e}_2$, $\mathbf{e}_3$) corresponds to the principal reference frame ($\mathbf{e}_I$, $\mathbf{e}_{II}$, $\mathbf{e}_{III}$) of the fibrous architectures. Second, the figure proves that

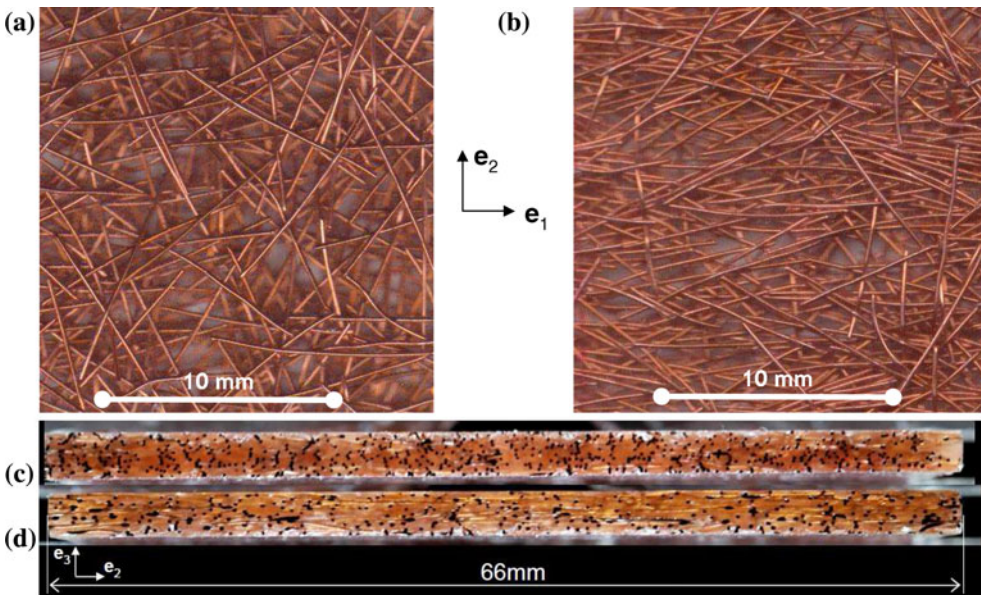

Fig. 2 2D optical micrographs of two model composite plates containing a volume fraction of fibres $\phi \approx 0.1$ and having a nearly planar random fibre orientation in ($\mathbf{e}_1$,$\mathbf{e}_2$) (a, d) or a preferred fibre orientation along the $\mathbf{e}_1$-direction (**b**, **c**). Micrographs **a**, **b** are top views parallel to $\mathbf{e}_3$, micrographs **c**, **d** are side views along $\mathbf{e}_1$

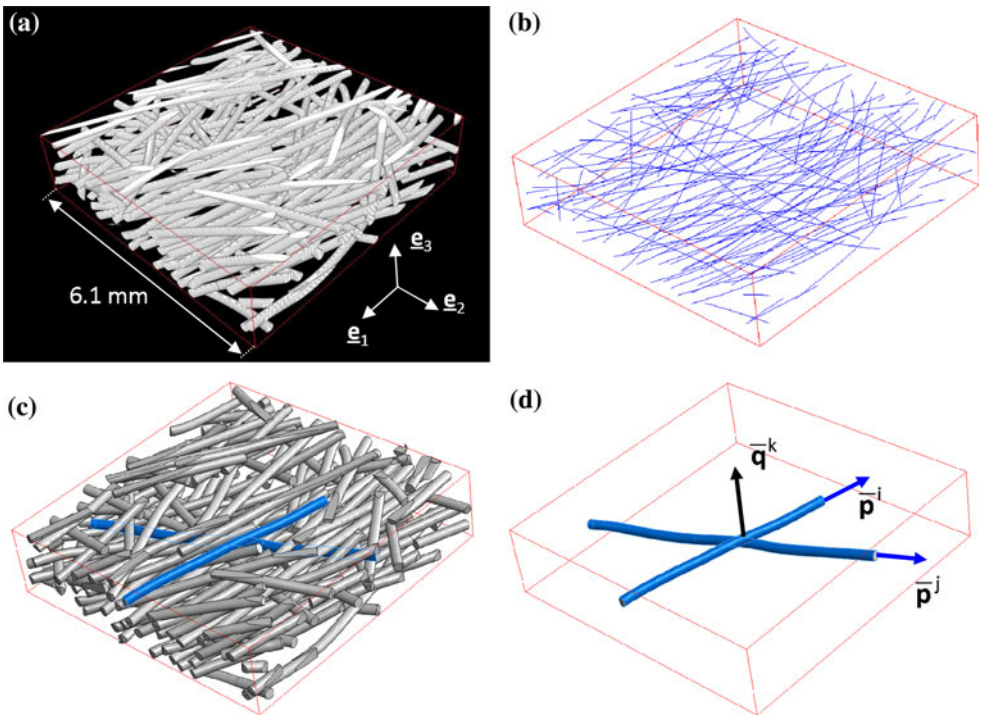

Fig. 3 Method used to estimate fibrous microstructure descriptors. From the segmented volume extracted from a 3D scanned volumes of a composite plate with preferred fibre orientation and $\phi = 0.17$ (**a**), the fibre centrelines are determined (**b**), then the fibrous network is numerically generated (**c**) so that fibre-fibre contacts k of normal unit vector $\overline{\mathbf{q}}^k$ between two fibres i and j (of mean unit orientation vectors $\overline{\mathbf{p}}^i$ and $\overline{\mathbf{p}}^j$) can be detected (d)

the fibre orientation vectors $\overline{\mathbf{p}}^i$ mainly lie in the mid-plane ($\mathbf{e}_1$,$\mathbf{e}_2$) of the plates (e.g. A_{33} is very small compared with A_{11} and A_{22}). Thus, from these results (confirmed for the other scanned volume), the fibre orientation in ($\mathbf{e}_1$,$\mathbf{e}_2$) of all the other (non-scanned) samples was characterised by using the 2D optical micrographs such as those shown in Fig. 2a, b and the software ImageJ. As presented in Dumont et al. [14], the projections of the vectors $\overline{\mathbf{p}}^i$ in ($\mathbf{e}_1$,$\mathbf{e}_2$) of $N = 120$ fibres were manually picked for each sample. By assuming that $A_{33} = A_{III} \approx 0.02$ (*cf.* Fig. 4a) and by using Eqs. 3, 9, it was possible to obtain estimations of the principal value A_I (the other value is such that $A_{II} = 1 - A_I - A_{III}$), φ_1, φ_2 and φ_3, for planar random and moderately orientated samples, respectively. These results are summarised in Table 2. They point out the reproducibility of the processing route used to manufacture the plates [14]. Despite the noticeable differences on the two types of studied fibre orientation, these results also show that the orientation function φ_3 does not vary significantly.

– Fibre–fibre contacts—The coordination number $\bar{Z}$ together with the orientation of fibre–fibre contacts in the plates were obtained with the algorithm developed in Latil et al. [24]. Thus, from the fibre centrelines shown in Fig. 3b, all the fibres contained in the scanned volumes were first generated numerically, as shown in Fig. 3c. Then, the location and the normal unit vector $\overline{\mathbf{q}}^k$ of each fibre-fibre contact k among the $\mathcal{N}$ contacts were calculated (a contact was considered as relevant each time a couple of regenerated fibres overlapped), as illustrated in Fig. 3d. An example of results obtained by following this procedure is illustrated in Fig. 4b. Then, estimations of the average coordination numbers in the plates could be obtained. For the example shown in Fig. 3a, i.e. for an orientated architecture with $\phi = 0.17, \bar{Z}$ reaches 13.5 ± 0.3, corresponding to a fibre coordination number per unit of length $z = 1350$ m^{-1} (the scattering takes into account possible errors induced during the determination of the fibre centre lines [24]). For the second scanned volume, i.e. for an nearly planar random architecture with $\phi = 0.10, \bar{Z}$ reaches 8.4 ± 0.3 ($z = 840$ m^{-1}). These results prove that the studied fibrous architectures belong to the concentrated regime since $\bar{Z} \neq 0$. Finally, as for the fibre orientation, it was also possible to analyse the orientation of the $\mathcal{N}$ contacts ($\mathcal{N} = 214$ in the example of Fig. 4c), either by using a unit sphere representation or the second-order orientation contact tensor $\mathbf{B}$ [24]:

$$\mathbf{B} = \frac{1}{\mathcal{N}} \sum_{k=1}^{\mathcal{N}} \overline{\mathbf{q}}^k \otimes \overline{\mathbf{q}}^k. \tag{11}$$

As shown in Fig. 4c, most of the normal vectors of fibre–fibre contacts are orientated along the $\mathbf{e}_3$-direction.

Characterisation of the in-plane conductivity

Experimental results concerning the in-plane thermal conductivity of the plates have been gathered in Fig. 5.

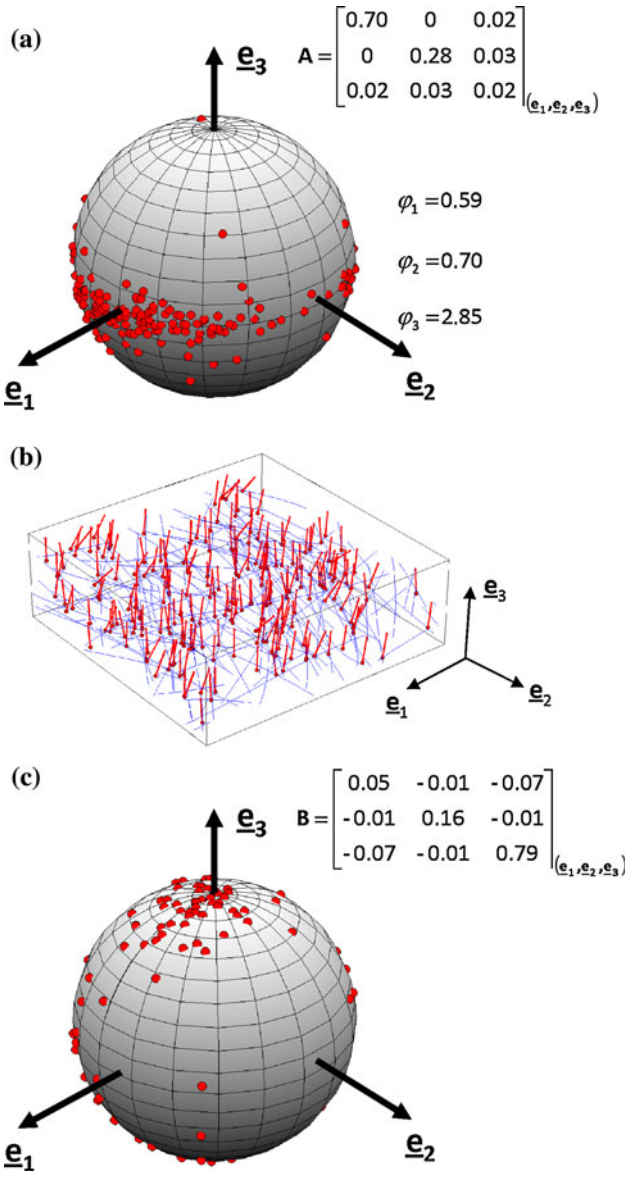

Fig. 4 Orientation of the fibres (**a**) and of the fibre-fibre contacts (**c**) in the volume (**b**) obtained from micrograph of figure 3(**a**)

Figure 5a shows the dimensionless in-plane effective conductivities $\Lambda_i^* = \Lambda_i/\lambda_m$ ($i = I, II$) as functions of the volume fraction of fibres ϕ. The graph (b) represents the evolution of the ratio Λ_i^*/A_i ($i = I, II$, no summation) with ϕ, where the values of the major components A_i of the orientation tensor **A** are obtained from Table 2. Some comments can be made about these results:

- Whatever the fibre orientation tensor **A**, Fig. 5a emphasises the very strong increase of the conductivities Λ_i^* with ϕ, in agreement with most of the literature results dealing with the thermal or electrical conductivities of conductive fibrous materials (e.g. [2, 10, 20, 39, 47]). For instance, the average thermal conductivity of the studied polymer composites is $\approx$40 times higher than the conductivity of the polymer matrix when the fibre content $\phi = 0.1$, this "thermal multiplication factor" reaches about 150 at $\phi = 0.24$ for orientated fibrous architectures.
- The fibre orientation induces a noticeable anisotropy of the effective conductivity, as mentioned in earlier studies for other conductive polymer composites [20, 47].

Table 2 Fibre orientation descriptors for the planar random and the orientated fibrous networks

Fibrous Architectures	A_I	φ_1	φ_2	φ_3
Planar random	0.49 ± 0.05	0.67 ± 0.01	0.61 ± 0.01	2.00 ± 0.5
Orientated	0.69 ± 0.05	0.61 ± 0.03	0.68 ± 0.03	2.35 ± 0.5

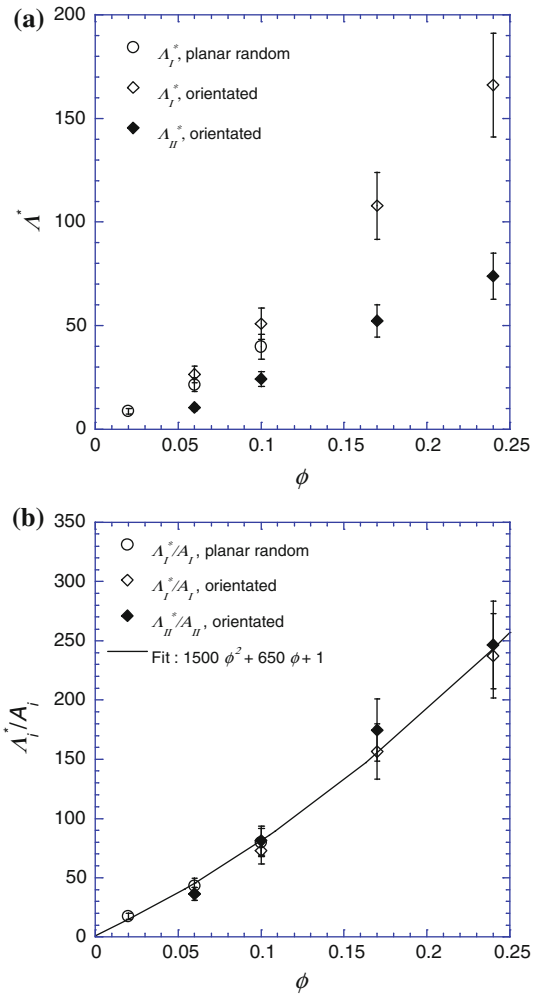

Fig. 5 Experimental results (*marks*) showing the evolution of the dimensionless effective thermal conductivities Λ_i^* with the volume fraction of fibres ϕ for different fibre orientations (**a**) and the evolution of the ratios Λ_i^*/A_i with the fibre content ϕ (**b**)

– Figure 5b shows that the anisotropy of the $\mathbf{\Lambda}$ is closely linked with that of $\mathbf{A}$. Indeed, given the fibre orientation, the ratios $\Lambda_{\mathrm{I}}^*/A_{\mathrm{I}}$ and $\Lambda_{\mathrm{II}}^*/A_{\mathrm{II}}$ are nearly identical, whatever the considered fibre content. Besides, whatever the fibre orientation, the ratios Λ_i^*/A_i follow a single master curve (see the continuous line):

$$\frac{\Lambda_i^*}{A_i} \approx 1500\phi^2 + 650\phi + 1. \tag{12}$$

This last expression allows us to better gauge the influence of the fibre content, whatever the fibre orientation. The second-order polynomial function that was used to fit the results exhibits a linear term and a quadratic one, in accordance with the general trend predicted with the proposed conduction model, see Eqs. 1, 2, 5, 7. It must be pointed out that these two terms are approximately of the same order of magnitude (see next section).

Comparison and discussion

Microstructure and conductivity measurements obtained in the two last sections are now discussed and compared with the predictions given by the analytical microstructure (Eq. 8) and conductivity (Eqs. 1, 2, 5, 7) models:

– The image analysis subroutines provided useful data about the geometry, position and orientation of fibres from the 3D scanned volumes. Fibres can be considered as straight slender rods, in line with the assumptions of the proposed conduction model. Besides, useful descriptors of the fibre orientation distibution were estimated. The first one is the second-order fibre orientation tensor $\mathbf{A}$ which is required to estimate the conduction contributions Eq. 2 and Eq. 5. The three others are the orientation functions φ_1, φ_2 and φ_3, which are useful to estimate the coordination number $\bar{Z}$ Eq. 8 and the conduction contribution Eq. 5. Thus, by using the values of these functions found for the two scanned volumes, the predicted coordination number equals 13.7 for the orientated architecture with $\phi = 0.17$ and 9.3 for the nearly planar random architecture with $\phi = 0.10$. These values are very close to those extracted directly from the same scanned volumes, i.e 13.5 and 8.4 (see, Characterisation of the fibrous architectures) These results tend to prove that the tube model, despite its strong assumptions (straight fibres, soft core assumption), can well predict the coordination numbers of the studied fibrous architectures. This latter should range between 1.8 and 20 when considering the whole set of studied microstructures.

– From the knowledge of the thermophysical properties of the matrix and the fibre (λ_{m}, λ_{f}), the fibre geometry (l_{f}, d_{f}), content (ϕ), orientation ($\mathbf{A}, \varphi_1, \varphi_2, \varphi_3$) and connectivity ($\bar{Z}$), it is now possible (i) to estimate the unique remaining constitutive parameter of the conduction model in Eqs. 1, 2, 5, 7, i.e. the contact conductance h_{c}, and (ii) to assess the relevance of the proposed conduction model. For the sake of simplicity, a single value h_{c} was identified, whatever the fibre content and orientation. Such a value was determined in order to obtain the best fit of the whole experiments: $h_{\mathrm{c}} = 1.7 \times 10^3\ \mathrm{Wm^{-2}K^{-1}}$. The comparison between the experimental data and the model predictions are summarised in Fig. 6, in which marks represent the experimental results and lines the model predictions. As shown in this figure, the proposed model, despite its simplicity, fits well the experimental data. Indeed, it can capture the influence of the fibre orientation (graph a) and the volume fraction of fibres (graph b). For graph (b), please notice that only the prediction given for

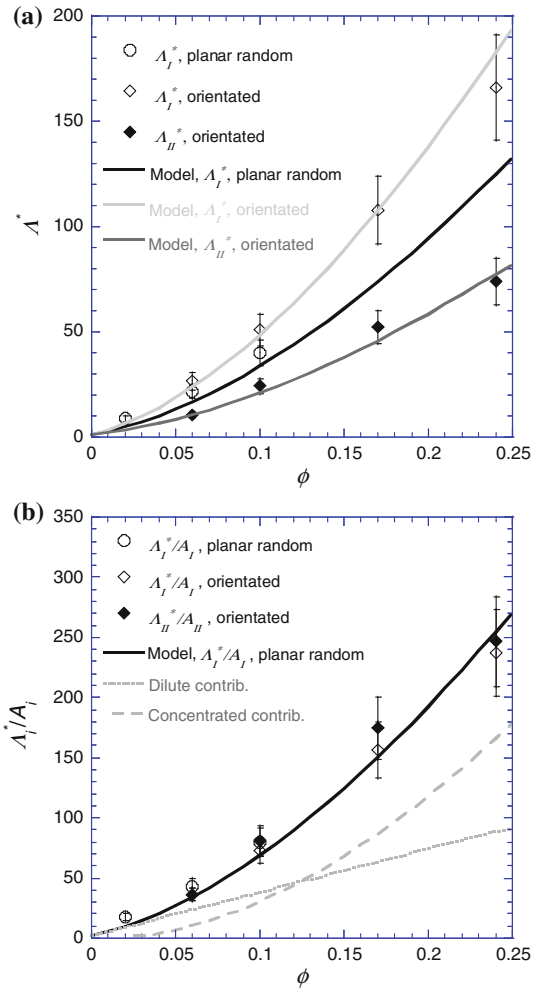

Fig. 6 Comparison experiments (*marks*)—model predictions (*lines*). Graph **a** dimensionless effective conductivity Λ^* as a function of the fibre content ϕ for planar random and orientated fibrous microstructures. Graph **b** ratios Λ_i^*/A_i as functions of ϕ (**b**). In this graph, the *grey lines* represent the dilute and the concentrated contributions to the overall conductivity represented by the *black line*

planar random microstructures was displayed, that obtained for oriented microstructures being nearly superimposed.

– The graph (a) in Fig. 7 represents the evolution of the resulting Biot number $\mathbb{B}$, see Eq. 4. As shown from this graph, whatever the investigated fibre orientations, $\mathbb{B}$ (i) is a decreasing function of the fibre content and (ii) ranges between 2×10^{-2} and 6×10^{-3}. The first point is mainly related to the increase of $\bar{Z}$ with ϕ (see Eq. 8), which in turn yields to a decrease of $\mathbb{B}$ (see Eq. 4). The second point, i.e. the moderate range of values of $\mathbb{B}$, tends to prove that both conduction inside the fibres $\mathbf{\Lambda}^{cI}$ and through fibre–fibre contacts $\mathbf{\Lambda}^{cIII}$ contribute to the overall conductivity of the considered fibrous networks $\mathbf{\Lambda}^{c}$ (see also [44]).

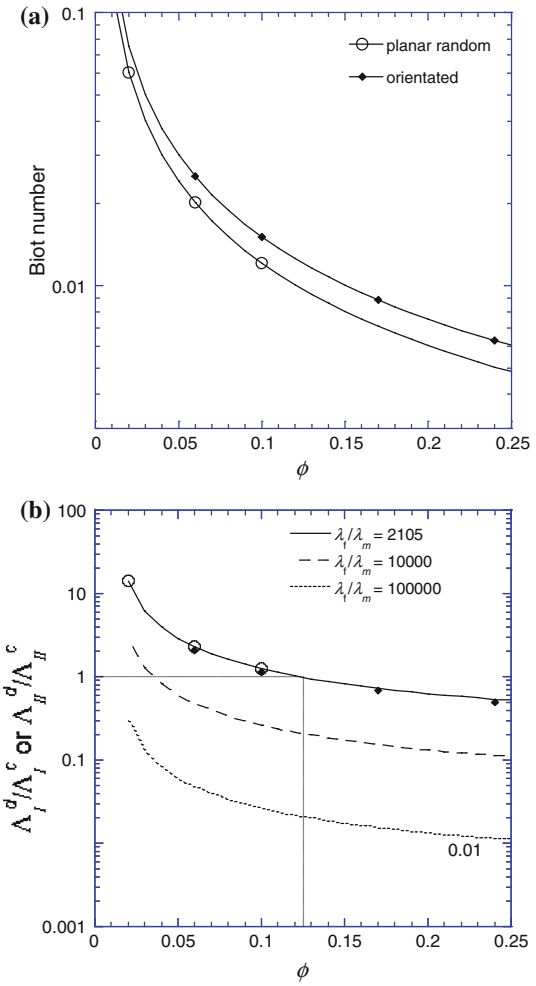

Fig. 7 **a** Estimation (4) of the Biot number as a function of ϕ for the different studied fibrous networks. In both graphs, marks correspond to the studied microstructures. **b** Estimation of the conductivity ratio $\Lambda_{\mathrm{I}}^{\mathrm{d}}/\Lambda_{\mathrm{I}}^{\mathrm{c}} \approx \Lambda_{\mathrm{II}}^{\mathrm{d}}/\Lambda_{\mathrm{II}}^{\mathrm{c}}$ with the fibre content for various local conductivity ratio $\lambda_{\mathrm{f}}/\lambda_{\mathrm{m}}$

– By using the estimated value of h_c, it is also possible to assess the magnitude of the two contributions $\mathbf{\Lambda}^{d}$ and $\mathbf{\Lambda}^{c}$ involved in Eq. 1. This is illustrated in the graph (b) of Fig. 6, but also in the graph (b) of Fig. 7, where the evolution of the ratios $\Lambda_{\mathrm{I}}^{\mathrm{d}}/\Lambda_{\mathrm{I}}^{\mathrm{c}} \approx \Lambda_{\mathrm{II}}^{\mathrm{d}}/\Lambda_{\mathrm{II}}^{\mathrm{c}}$ with the fibre content ϕ is given. The marks and the continuous line shown in this graph correspond to the studied composite plates, i.e. to a local conductivity ratio $\lambda_{\mathrm{f}}/\lambda_{\mathrm{m}} \approx 2100$. Heat transfers in the bulk matrix should play a leading role at fibre contents below ≈ 0.125. At this fibre content, both contributions are expected to be of the same order of magnitude. As ϕ is further increased, the fibre contacts should gain preponderance and should contribute to $\approx 66\%$ of the overall conductivity at $\phi = 0.24$. Hence, these graphs show that heat transfers in the bulk matrix should not be neglected, even if the considered fibrous microstructures are fully connected and if $\lambda_{\mathrm{f}}/\lambda_{\mathrm{m}}$ is high. Figure 7 also plots the evolution of the ratios $\Lambda_{\mathrm{I}}^{\mathrm{d}}/\Lambda_{\mathrm{I}}^{\mathrm{c}} \approx \Lambda_{\mathrm{II}}^{\mathrm{d}}/\Lambda_{\mathrm{II}}^{\mathrm{c}}$, for higher local conductivity ratios, respectively, 10^4 and 10^5 (all the other physical and microstructure parameters being kept constant). As expected, increasing $\lambda_{\mathrm{f}}/\lambda_{\mathrm{m}}$ should induce a decrease of heat transfers in the matrix. When $\lambda_{\mathrm{f}}/\lambda_{\mathrm{m}} = 10^4$, such a contribution should still represent from 38 to 9% of the overall in-plane conductivity as ϕ increases from 0.05 to 0.24. When $\lambda_{\mathrm{f}}/\lambda_{\mathrm{m}} = 10^5$, it should be fair to assume that $\mathbf{\Lambda} \approx \mathbf{\Lambda}^{c}$, the other contribution only representing ≈ 5–1% as ϕ goes from 0.05 to 0.24.

Conclusion

We measured the in-plane conductivity of polymer composites plates reinforced with conductive and architectured copper fibres. In order to circumvent the experimental difficulties often encountered in the literature, particular attention was paid to (i) process composites plates with controlled fibrous microstructures and (ii) limit experimental artefacts during thermal conductivity measurements. Special attention was also paid to finely characterise the as-processed microstructures, showing that fibres are rather straight and have planar orientations. The average fibre coordination number, i.e. the avergage number of fibre–fibre contacts per fibre, could also be estimated for two samples, showing that fibres exhibit multiple fibre–fibre contacts. Likewise, the components of the in-plane conductivity tensor of the tested plates are found to be second-order polynomial functions of the fibre content and the anisotropy of the conductivity tensor is closely linked with the second-order fibre orientation tensor.

An analytical model for in-plane conductivity was proposed from different literature models: a fibre coordination model based on soft core assumptions and two conduction models proposed for slender and highly conductive straight fibres which account for the involved in-plane conduction mechanisms. It was first shown that the fibre coordination model could correctly predict the coordination numbers found experimentally. Thereupon, it was shown that the model predictions fit well the conductivity measurements, in turn that conduction within the matrix should be taken into account: such a mechanism can be neglected only in the cases of very high-conductivity ratios between the fibres and the matrix.

By combining the 3D description of the fibrous architecture provided by the X-ray microtomography and by following the guidelines proposed in Vassal et al. [43], work in progress is now focusing on extending the present model, which is restricted to networks of rather straight fibres, to fibrous media made up of slender, wavy and entangled fibres.

References

1. Advani SG, Tucker CL (1987) J Rheol 3(8):751
2. Agari Y, Ueda A, Nagai S (1991) J Appl Polym Sci 43:1117
3. Assael MJ, Botsios S, Gialou K, Metaxa IN (2005) Int J Thermophys 26:1595
4. Assael MJ, Antoniadis KD, Tzetzis D (2008) Compos Sci Technol 68:3178
5. Auriault J-L (1983) Int J Heat Mass Trans 26(6):861
6. Batchelor G, O'Brien F, O'Brien R (1977) Proc R Soc Lond A 355:313
7. Carson J, Lovatt S, Tanner D, Cleland AC (2005) Int J Heat Mass Trans 48:2150
8. Cheng X, Sastry A (1999) Mech Mater 31:765
9. Cheng X, Sastry A, Layton BE (2001) ASME J Eng Mater Technol 123:12
10. Dalmas F, Dendievel R, Chazeau L, Cavaillé J-Y, Gauthier C (2006) Acta Mater 54:2923
11. Danès F, Garnier B, Dupuis T (2003) Int J Thermophys 24:771–784
12. Danès F, Garnier B, Dupuis T, Lerendu P, Nguyen T-P (2005) Compos Sci Technol 65:945
13. Doi M, Edwards SF (1978) J Chem Soc Faraday Trans II 74(1):560
14. Dumont P, Vassal J-P, Orgéas L, Michaud V, Favier D, Månson JA-E (2007) Rheol Acta 46:639
15. Eberhardt C, Clarke A (2002) J Microscopy 206:41
16. Faessel M, Delisée C, Bos F, Castéra P (2005) Compos Sci Technol 65:1931
17. Favier V, Dendievel R, Canova G, Cavaillé J-Y, Gilormini P (1997) Acta Mater 45:1557
18. Flandin L, Verdier M, Boutherin B, Brechet Y, Cavaillé J-Y (1999) J Polym Sci B 37:805
19. Kaviany M (1991) In: Principles of heat transfer in porous media. Springer, New York
20. Keith J, Hingst C, Miller M, King J, Hauser R (2006) Polym Compos 27:388–394
21. Kim I, Torquato S (1993) J Appl Phys 74:1844
22. Kim Y, Hayashi T, Endo M, Gotoh Y, Wada N, Seiyama J (2006) Scr Mater 54:31
23. Kirkpatrick S (1973) Rev Mod Phys 45:574
24. Latil P, Orgéas L, Geindreau C, Dumont PJJ, Rolland du Roscoat S (2011) Compos Sci Technol 71:480
25. Le TH, Dumont PJJ, Orgéas L, Favier D, Salvo L, Boller E (2008) Compos Part A 39:91–103
26. Le Corre S, Dumont P, Orgéas L, Favier D (2005) J Rheol 49:1029
27. Masse J, Salvo L, Rodney D, Brechet Y, Bouaziz O (2006) Scripta Mater 54:1379
28. Milton G (2002) The theory of composites. Cambridge University Press, Cambridge
29. Néda Z, Florian R, Bréchet Y (1999) Phys Rev E 59:3717
30. Ouyang Z, Zhang F, Wang L, Favro LD, Thomas RL (1998) In: Thomson DO, Chimenti DE (eds) Review of progress in quantitative nondestructive evaluation. Plenum Press, New York, p 453
31. Petrich MP, Koch DL, Cohen C (2000) J Non-Newtonian Fluid Mech 95:101
32. Philippi I, Bastale JC, Maillet D, Degiovanni A (1995) Rev Sci Instrum 66:182
33. Ranganathan S, Advani SG (1991) J Rheol 35:1499
34. Rocha A, Acrivos A (1973) Q J Mech Appl Math 26:441
35. Rolland du Roscoat S, Decain M, Thibault X, Geindreau C, Bloch J-F (2007) Acta Mater 55:2841
36. Sahimi M (2003) In: Heterogeneous materials, vols I and II. Springer-Verlag, New York
37. Sundararajakumar RR, Koch DL (1997) J Non-Newtonian Fluid Mech 73:205
38. Sweeting R, Liu X (2004) Compos Part A 35:933
39. Tekce H, Kumlutas D, Tavman I (2007) J Reinf Plast Compos 26:113
40. Toll S (1993) J Rheol 37(1):123
41. Torquato S (2001) In: Random heterogeneous materials. Springer-Verlag, New York
42. Vassal J-P, Orgéas L, Favier D, Auriault J-L, Le Corre S (2008a) Phys Rev E 77:011302
43. Vassal J-P, Orgéas L, Favier D, Auriault J-L, Le Corre S (2008b) Phys Rev E 77:011303
44. Vassal J-P, Orgéas L, Favier D (2008c) Model Simul Mater Sci Eng 16:035007
45. Volkov AN, Zhigilei LV (2011) Phys Rev Lett 104:215902
46. Wang C, Cook KA, Sastry AM (2003) J Electrochem Soc 150:385
47. Weber M, Kamal M (1997) Polym Compos 18:711
48. Webman I, Jornter J, Cohen M (1975) Phys Rev B 11:2885
49. Yasuda K, Mori N, Nakamura K (2002) Int J Eng Sci 40:1037